Mechanism of action of a flavin-containing monooxygenase

Subramaniam Eswaramoorthy*, Jeffrey B. Bonanno†, Stephen K. Burley‡, and Subramanyam Swaminathan*§

*Biology Department, Brookhaven National Laboratory, Upton, NY 11973; †New York Structural Biology Center, New York, NY 10027; and ‡SGX Pharmaceuticals, Inc., San Diego, CA 92121

Edited by Brian W. Matthews, University of Oregon, Eugene, OR, and approved May 11, 2006 (received for review March 24, 2006)

Elimination of nonnutritional and insoluble compounds is a critical task for any living organism. Flavin-containing monooxygenases (FMOs) attach an oxygen atom to the insoluble nucleophilic compounds to increase solubility and thereby increase excretion. Here we analyze the functional mechanism of FMO from *Schizosaccharomyces pombe* using the crystal structures of the wild type and protein–cofactor and protein–substrate complexes. The structure of the wild-type FMO revealed that the prosthetic group FAD is an integral part of the protein. FMO needs NADPH as a cofactor in addition to the prosthetic group for its catalytic activity. Structures of the protein–cofactor and protein–substrate complexes provide insights into mechanism of action. We propose that FMOs exist in the cell as a complex with a reduced form of the prosthetic group and NADPH cofactor, readying them to act on substrates. The 4α-hydroperoxyflavin form of the prosthetic group represents a transient intermediate of the monooxygenation process. The oxygenated and reduced forms of the prosthetic group help stabilize interactions with cofactor and substrate alternately to permit continuous enzyme turnover.

three-dimensional structure | xenobiotics | methimazole

Flavin-containing monooxygenases (FMOs) and cytochromes P450 are two important microsomal proteins involved in the process of nonnutritional foreign compounds metabolism known as xenobiotics. Their main function is to add molecular oxygen to lipophilic compounds, making them soluble to ensure rapid excretion. FMOs oxygenate nucleophilic O, N, S, and Se atoms of a wide range of substrates, such as amines, amides, thiols, and sulfides (1). FMOs of liver microsomes are known as microsomal FMOs (2). They are divided into three classes, namely FMOs, *N*-hydroxylating monooxygenases, and Baeyer–Villigar monooxygenases (BVMOs). The signature sequence, FXGXXXHXXXW(P/D), of BVMO differs from FXGXXXHXXX(Y/F) of FMO, distinguishing these two enzymes (3). The mechanism of action of FMOs is distinctly different from that of other monooxygenases. FMOs do not require substrate for dioxygen reduction of the prosthetic group FAD by NADPH. Instead, the protein plus the prosthetic group and the cofactor in its 4α-hydroperoxyflavin form stand ready to perform chemistry on available nucleophiles (4).

The mammalian FMO gene family contains five similar genes (FMO1 through FMO5). FMO1 and FMO3 are prominent isoforms expressed mainly in liver microsomes and in other tissues. FMO1 expression is higher in fetal liver, whereas FMO3 is more abundant in adult human. FMO2 is expressed in the lungs of nonhuman primates; FMO4 and FMO5 represent scarce isoforms (5, 6). Individuals with defective FMOs exhibit "fish odor syndrome" caused by excretion of trimethylamine instead of its oxygenated form, trimethylamine *N*-oxide in urine, sweat, and breath (7).

Here we present three crystal structures, (*i*) FMO from *Schizosaccharomyces pombe* with a bound FAD, (*ii*) its complex with NADPH, and (*iii*) an enzyme–substrate [*N*-methyl-2-mercaptoimidazole (methimazole)] complex. Hydride ion reduction of FAD to $FADH_2$ and the mechanism of oxygenation of the substrate methimazole are discussed.

Results

FMO Activity. The protein solution appeared dark yellow, possibly arising from the prosthetic group FAD. On adding NADPH it turned pale yellow, apparently because of the FAD reduction to $FADH_2$. The protein and NADPH complex was added to the aerated tricine reaction buffer. The protein was in the active form at this stage and ready to oxygenate a suitable substrate (methimazole in this case). The 5,5′-dithiobis(2-nitrobenzoate) (DTNB) added to the reaction mixture was reduced to nitro-5-thiobenzoate by DTT. OD was measured at 412 nm every 5 seconds to monitor the DTNB concentration. OD values decreased with time for ≈5 min and stabilized. Although the DTNB was reduced by DTT, there was residual OD observed after 5 min. Methimazole was added to the reaction mixture at this point, and the OD measurement was started. The OD increased steadily for ≈10 min and stabilized.

Dixit and Roche (1) have demonstrated that oxygenated methimazole reacts with nitro-5-thiobenzoate to produce DTNB. The increase in OD corresponds to the increment of DTNB in the reaction mixture, confirming oxygenation of substrate. This reaction also demonstrated that the maximum DTNB production was achieved within 10 min. In the control experiment without methimazole, the OD increased very slowly. It took ≈30 min to reach the maximum OD of 1.12, which is considerably less than that of the experiment with methimazole (1.32). The difference in OD reading between these two experiments (with and without methimazole) over 10 min is plotted in Fig. 1.

Structure of FMO. The crystal structure of the enzyme–FAD complex was first determined as part of the structural genomics effort by the New York SGX Research Consortium and has been deposited in the Protein Data Bank (PDB ID code 1VQW). The structural models of enzyme–FAD, enzyme–FAD–NADPH, and enzyme–FAD–methimazole complexes contain residues Leu-3 to Glu-444. No electron density was observed for the two N-terminal residues, the three C-terminal residues, and the C-terminal hexahistidine affinity tag. The electron density maps were of high quality for the entire model, and the protein exists as dimer (Fig. 5, which is published as supporting information on the PNAS web site). Whereas the enzyme–FAD and enzyme–FAD–NADPH complex structures have one dimer per unit cell of the P1 symmetry, the enzyme–FAD–methimazole complex has two. No conformational changes were evident when the three structures were compared in detail, permitting refinement with noncrystallographic symmetry restraints.

FMO (447 aa) is composed of two structural domains (Fig. 2). Residues 176–291 form a small structural domain (hereafter called

---

Conflict of interest statement: No conflicts declared.

This paper was submitted directly (Track II) to the PNAS office.

Abbreviations: FMO, flavin-containing monooxygenase; methimazole, *N*-methyl-2-mercaptoimidazole; DTNB, 5,5′-dithiobis(2-nitrobenzoate); BVMO, Baeyer–Villigar monooxygenase.

Data deposition: The atomic coordinates and structure factors have been deposited in the Protein Data Bank, www.pdb.org (PDB ID codes 1VQW, 2GV8, and 2GVC).

§To whom correspondence should be addressed. E-mail: swami@bnl.gov.

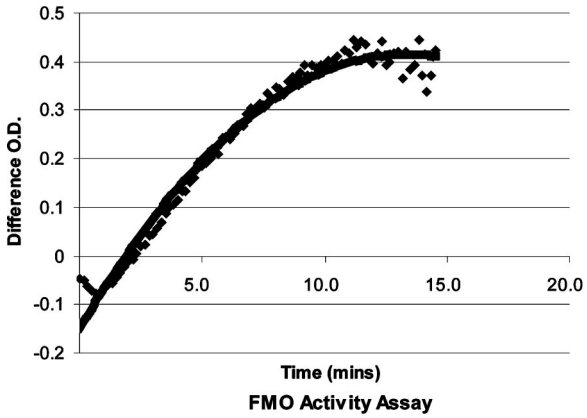

Fig. 1. FMO activity assay. The OD reading at 412 nm due to the DTNB formation in the presence of the substrate methimazole is plotted against time. Dots represent experimental points, and the smoothened curve is given as a solid line. Oxygenated substrate formation is confirmed by this experiment.

the insertion domain), with the remainder of the polypeptide chain forming a larger single domain. A channel is present between these two domains. A 60-residue-long polypeptide chain segment in a predominantly random coil configuration with some minor secondary structure elements occurs in the interface between the two domains, where it appears to stabilize the overall domain organization.

The FMO large domain consists of a four-stranded parallel β-sheet flanked by a three-stranded antiparallel β-sheet on one side and six α-helices on the other (Fig. 6, which is published as supporting information on the PNAS web site). The insertion domain consists of a five-stranded parallel β-sheet flanked by a three-stranded antiparallel β-sheet and a helix on one side, and an α-helix on the other. The C terminus of the polypeptide chain forms a bent helix ($\alpha 8_1$ and $\alpha 8_2$) that extends from the large domain to the insertion domain. The C termini of the parallel β-sheets of the two domains point toward each other. This structure also contains three strand–turn–helix motifs. The first motif is formed by $\beta 1$ and $\alpha 1$. This motif has a nucleotide binding sequence, GAGPSG (GXGXXG), which stabilizes binding of FAD in all three structures presented here. The second motif, formed by $\beta 8$ and $\alpha 4$, is located in the insertion domain, where it stabilizes binding of NADPH in the enzyme–FAD–NADPH complex (Fig. 7, which is published as supporting information on the PNAS web site). In the enzyme–FAD–substrate complex, methimazole replaces NADPH and occupies the nicotinamide site. The third strand–turn–helix motif, formed by $\beta 15$ and $\alpha 5$, occurs where the C terminus of the insertion domain connects to large domain. The second half of the large domain contains the FMO identifying sequence FXGXXXHXXXF and interacts with the flavin part of FAD.

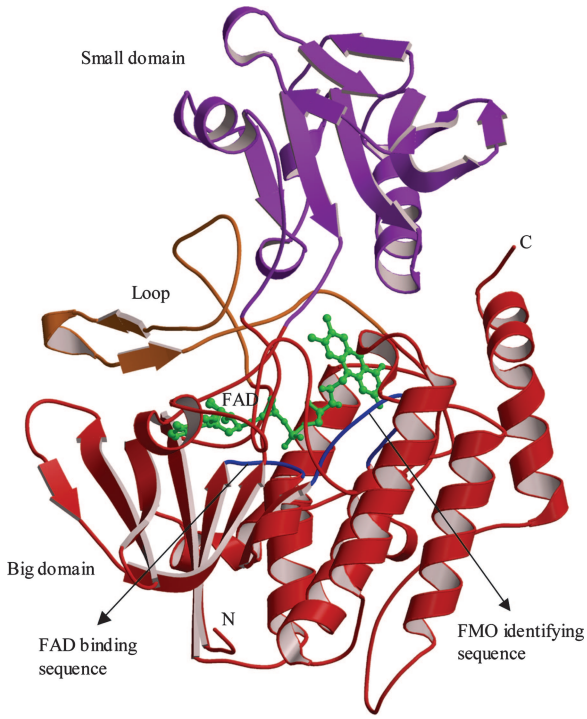

Fig. 2. Ribbon representation of the protein and ball-and-stick model of FAD. The strand–turn–helix motifs and the loop interlinking the two domains are labeled. FAD is in the large domain and has no interaction with the small domain.

FAD Binding. There is a channel between the two domains with a shallow depression on the surface of the large domain. The prosthetic group, FAD, is located in the channel along the depression and interacts only with the large domain (Fig. 3*a*). The nucleotide-binding motif GAGPSG located in the first strand–turn–helix motif is at the core of the large domain bordering the shallow depression. The adenine nucleotide makes hydrogen-bonding contacts with this motif. Atom N3 of adenine is hydrogen-bonded to the main-chain nitrogen of Arg-39, and the base is stacked with the guanidine group of Arg-39. The flavin phosphate is anchored to the GAGPSG motif together with a bound water molecule. This well localized water molecule is hydrogen-bonded with the nitrogen atoms of Gly-15 and Gly-18, the carbonyl oxygen of Cys-172, and OP1 of the flavin phosphate. A number of water molecules surrounding the phosphates mediate protein contacts. The oxygen atoms of the ribitol group also interact with the large domain via water molecules. The other nucleotide, flavin, extends toward the bulk solvent region and is exposed as observed in the enzyme–FAD complex (Fig. 3*b*). The prosthetic group is enveloped by the large domain together with a network of water molecules. N3 and O4 of the isoalloxazine ring form a hydrogen bond with protein atoms OG1 of Thr-92 and the main-chain nitrogen of Asn-91 (Table 1).

NADPH Binding. The crystal structure of the enzyme–FAD–NADPH complex showed NADPH bound to the protein in addition to FAD. FAD binding to this ternary complex is identical to that observed in the enzyme–FAD binary complex. Virtually all water molecules bridging between the enzyme and FAD in the binary complex are maintained in the ternary complex (Table 1). The NADPH cofactor is bound to the second nucleotide-binding motif, GGASSA, which is located at the strand–turn–helix motif within the insertion domain. Whereas FAD appears strongly bound to the enzyme, NADPH appears more loosely bound in a superficial shallow groove (Fig. 3*c*). The adenine portion of the cofactor interacts with the protein, whereas the nicotinamide extends toward the flavin moiety of FAD (Fig. 3*d* and Table 2).

The bases of nicotinamide and flavin interact with each other. Specifically, the nicotinamide is stacked with the isoalloxazine ring of the FAD, and atom O7 hydrogen bonds to N5 of the isoalloxazine ring. Oxygen atoms O2 and O3 of the nicotinamide sugar moiety are hydrogen-bonded to OD1 of Asn-91 and OH of Tyr-176. The phosphate attached to the adenine base is exposed to the solvent and does not appear to interact with the protein.

Methimazole Binding. Crystals of the enzyme–FAD–substrate complex were obtained from the solution containing protein with FAD, NADPH, and methimazole, and a quaternary complex was expected. It is remarkable that only methimazole and FAD are present in the structure, whereas NADPH is absent. The mode of

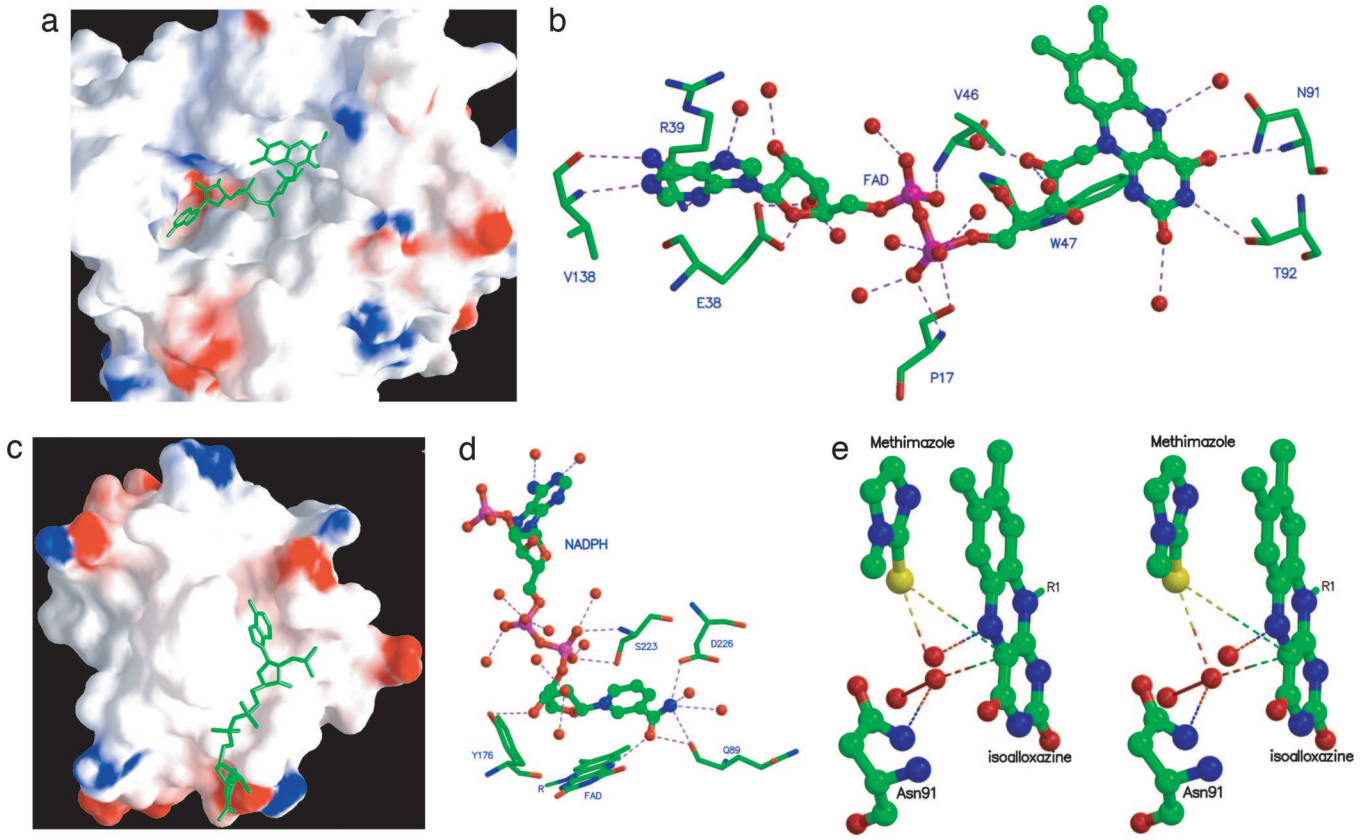

Fig. 3. Protein–cofactor and protein–substrate interactions. (*a*) Electrostatic potential of the large domain of FMO. The insertion domain was excluded to clarify the view of the cavity formed along the large domain. FAD is depicted as a stick model. This cavity accommodates the prosthetic group, with adenine completely buried in the protein, and the flavin is more exposed to the solvent. (*b*) Hydrogen bonding interactions of the prosthetic group. FAD is represented as a ball-and-stick model, and the protein residues are shown as sticks. Water molecules are shown as red spheres. (*c*) Electrostatic potential of the insertion domain of FMO. The NADPH cofactor is shown as a stick model. NADPH is bound to the protein in a shallow cavity. (*d*) Hydrogen bonding interactions of the cofactor. NADPH is rendered as a ball-and-stick model, and the protein residues are shown as sticks. Water molecules are shown as red spheres. (*e*) Stereo diagram of methimazole and the isoalloxazine ring stacking along with a nearby water molecule and Asn-91. The hydrogen bonding interactions are shown by dashed lines. Long dashed lines represent the possible interaction routes involved in the oxygen transfer to the substrate. Two water molecules bonded with a solid line represent the molecular oxygen.

FAD binding is the same as that observed for the wild-type protein. We believe that methimazole competes with the NADPH cofactor and replaces it. Methimazole occupies the nicotinamide binding position seen in the enzyme–FAD–NADPH complex and stacks with the isoalloxazine ring. It was previously thought that FMO forms a functional quaternary complex. Our results clearly show that the cofactor and substrate occupy overlapping binding sites by stacking on the FAD, thereby precluding quaternary complex formation. Methimazole is surrounded by water molecules and does not make any direct contacts with the protein.

In our initial refinement models, an elongated electron density feature positioned 3.7 Å from the S of methimazole was interpreted as a water molecule hydrogen-bonded to OD1 of Asn-91. However, the elongated electron density feature suggested the presence of a dioxygen molecule. When O_2 was modeled into this feature, the refinement converged well (Fig. 3*e*). It is, however, possible that this feature can be explained by one or more disordered water molecules.

Discussion

The biochemical assay of methimazole oxygenation unambiguously showed that this protein SPBP16F5.08c of *S. pombe* (Gen Bank accession no. GI: 19112574) is an FMO (8).

The structure of the wild-type protein is the first and the only one determined from the FMO protein family and will be useful as a representative model of this family. Cytochrome P450s contain heme as a prosthetic group, whereas FMOs use FAD. These proteins need a cofactor NADPH in addition to the prosthetic group to accomplish their functional goal. The structure includes two similar structural domains with the C-terminal portion of the parallel β-sheets facing each other. These β-sheets hold the prosthetic group (FAD) and the cofactor (NADPH), allowing them to interact for FAD reduction. The helical bundle found within the large domain may be responsible for substrate capture, although the role played by the FMO identifying sequence (FXGXXXHXXXF) is not clear.

Mechanism of FMO Activity. The catalytic activity of this enzyme is carried out mainly through the prosthetic group FAD and cofactor NADPH. Asn-91 is the only protein residue directly involved in the catalytic mechanism as substantiated from the crystal structures. To the best of our knowledge, this is the first study to elucidate the mechanism of action of FMO via crystallographic studies of distinct steps in the reaction pathway (Fig. 4).

FAD is a major electron carrier in the oxidation–reduction processes catalyzed by enzymes. The electron donor in most of reductive biosyntheses is NADPH, a reducing species that is readily available in the cells. In the process of monooxygenation by the enzyme FMO, the prosthetic group FAD is first reduced to $FADH_2$ through a hydride ion transfer from NADPH. In the second step $FADH_2$ accepts a molecular oxygen at the C4A (or C10) position of the isoalloxazine ring and becomes 4α-hydroperoxyflavin, FAD-

Table 1. Hydrogen bonding interactions of FAD in the wild-type and NADPH complex structures

FAD	Protein	Distance, Å	
		Wild type	NADPH
Adenine			
N1′	N Val-138	3.00	2.95
	OD1 Asp-137	2.96	3.19
N3′	N Arg-39	2.89	3.06
N6′	O Val-138	3.08	3.16
N7′	O Wat	2.93	3.06
O2	O Wat	2.43	2.83
	OE2 Glu-38	3.30	3.07
O3	O Wat	2.84	2.86
	OE1 Glu-38	2.47	2.58
	OE2 Glu-38	2.62	2.92
	NH1 Arg-40	3.00	3.08
Phosphates			
O1′	O Wat	2.62	2.83
	O Wat	3.25	3.03
	O Wat	—	2.95
O2′	N Val-46	2.95	2.99
	O4* Ribitol	2.76	2.69
O1P	O Wat	2.42	2.60
	N Ser-17	2.77	2.82
O2P	O Wat	2.99	2.72
	O Wat	3.06	2.87
	OG Ser-17	2.55	2.67
Ribitol			
O3*	NE1 Trp-47	2.81	2.98
O2*	O Wat	2.26	2.98
	O Wat	3.17	2.80
Flavin			
O2	O Wat	2.81	2.89
N3	OG1 Thr-92	3.21	2.94
O4	O7 NDP	n/a	3.16
	N Asn-91	3.15	3.02
N5	O7 NDP	n/a	3.05
	O Wat	3.15	n/a

Table 2. Hydrogen bonding interactions of NADPH in the NADPH complex structure

NADPH	Protein	Distance, Å
Adenine		
N1′	O Wat	2.99
N3′	O Wat	2.89
N6′	O Wat	3.10
Phosphates		
O1′	O Wat	2.55
	O Wat	2.77
O2′	O Wat	2.81
O1	O Wat	2.69
	N Ser-223	2.89
O2	O Wat	2.72
	OG Ser-223	2.82
Nicotinamide		
O2*	O Wat	3.08
	O Wat	2.61
	OD1 Asn-91	2.97
O3*	OH Tyr-176	3.17
N7	O Wat	3.03
	O Wat	3.19
	O Gln-89	3.07
	OD2 Asp-226	2.87
O7	N5 FAD	3.05
	O4 FAD	3.20
	O Gln-89	2.99

OOH. When a suitable substrate with a nucleophilic atom, such as the S in methimazole, binds productively to the protein/FAD-OOH complex, it is oxygenated to SO through the OOH moiety. A water molecule is released during this reaction, and the substrate becomes oxygenated as depicted in Fig. 4 (4, 9).

All three structures presented here contain the prosthetic group (FAD) bound to the first nucleotide binding motif and a modeled dioxygen molecule in dihydrogen peroxide form. The enzyme–FAD–NADPH complex structure showed the cofactor bound to the second nucleotide-binding motif located within the insertion domain. Interactions between FAD and NADPH are well defined in the electron density maps. The nicotinamide portion of NADPH stacks with the flavin of FAD in a novel fashion. Atom C2 of the nicotinamide base is 3.35 Å from N5 of the isoalloxazine ring. We propose that the hydride ion transfer takes place through these two atoms. The NH group (N5) of the reduced flavin moiety makes a hydrogen bond with O7 (3.08 Å) of the nicotinamide. In the enzyme–FAD–NADPH complex the prosthetic group exists in the reduced form ($FADH_2$) and the cofactor in a protonated form (NADP+) as given in step 3 of Fig. 4. We suggest that the enzyme exists with $FADH_2$ and NADP+ bound state in the cell.

At this stage the prosthetic group $FADH_2$ is ready to accept molecular oxygen. An electron density feature consistent with a bound oxygen molecule hydrogen-bonded to Asn-91 was observed in all three structures presented here. This molecular oxygen is located near the isoalloxazine ring and would be readily available for 4α-hydroperoxyflavin formation. When an appropriate substrate, such as methimazole, approaches the protein active site it replaces NADP+ and stacks with the isoalloxazine ring similarly positioned as compared with the sugar moiety of the nicotinamide (Fig. 3*e*). Both NADPH and methimazole interact with the same side of the isoalloxazine ring, and the substrate is able to compete and replace NADP+ as seen in the ternary complex structures. The methimazole complex structure has methimazole bound to the protein in the vicinity of the modeled molecular oxygen hydrogen-bonded to Asn-91. This molecular oxygen could bind to C4A (or C10) of the isoalloxazine ring and then undergo rapid transfer to substrate. Our crystal structure did not show molecular oxygen covalently bound to the isoalloxazine ring. Instead, the structure shows simultaneous binding of molecular oxygen and methimazole. This observation suggests that a molecular oxygen-bound prosthetic group represents an intermediate step in the oxygenation reaction pathway (step 4 of Fig. 4).

The dioxygen molecule was refined as a dihydrogen peroxide with the distance between the two oxygen atoms of 1.46 Å. The dioxygen could have been present in the enzyme. Atom O1 of this dioxygen molecule is at a distance of 3.7, 3.5, and 3.0 Å from C4A and C10 of isoalloxazine and ND2 of Asn-91, respectively. Hence, residue Asn-91 could play a critical role by supplying molecular oxygen to the isoalloxazine ring. The observation of dioxygen molecules near enzyme active sites is precedented in other structures (10, 11). Dioxygen is associated with metal atoms in naphthalene dioxygenase and cytochromes P450 (10, 12). The proposed dioxygen in this FMO structure is bound to Asn-91. The refined temperature factor of the dioxygen is 49.4 $Å^2$, whereas the average value for the protein model is 25.9 $Å^2$. The S atom of the methimazole is 4.8 Å from C4A and 4.5 Å from C10 atoms of the isoalloxazine ring. There is no indication that the isoalloxazine ring is present in the hydroperoxy form.

Once the substrate is oxygenated and a water molecule is released, FAD is regenerated from $FADH_2$ and is ready for another catalytic cycle. Our structures suggest that the cofactor and the substrate interact with the prosthetic group alternately, rendering the enzyme capable of oxygenating substrates continuously. Our finding suggests that the FAD reduction takes place before substrate binding but that the dioxygen acceptance occurs only in the presence of the substrate.

BIOCHEMISTRY

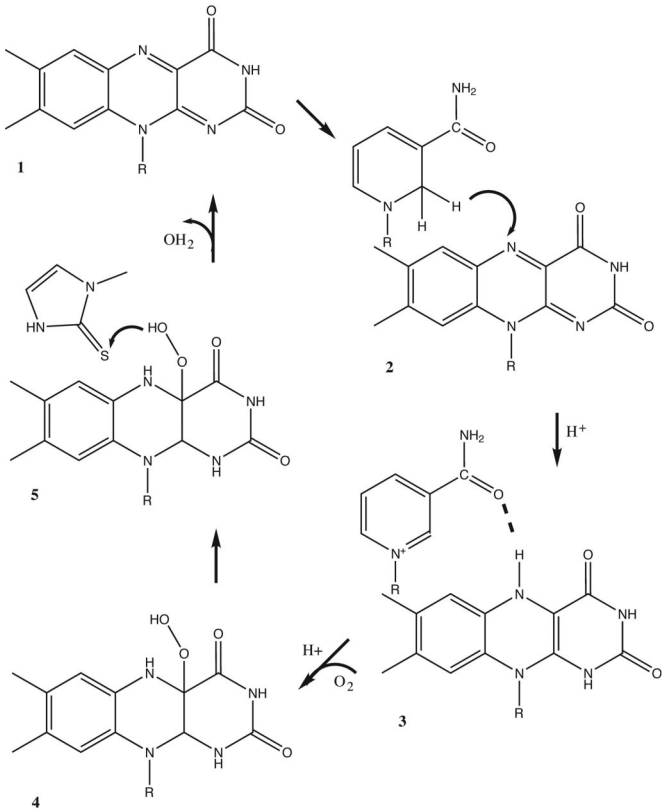

Fig. 4. Schematic representation of the functional mechanism of FMO. Only the relevant parts required to explain the function, isoalloxazine, nicotinamide, and methimazole, are shown. Step 1 is seen in the wild type, step 3 is seen in the protein–cofactor complex, and step 5 is seen in the protein–methimazole complex structures.

Table 3. Crystallographic data

	Wild type	NADPH complex	Substrate complex
Space group	P1	P1	P1
Unit cell			
a, Å	59.59	59.31	72.70
b, Å	72.64	72.53	84.45
c, Å	80.35	80.37	113.51
α, °	99.0	98.5	107.7
β, °	107.1	107.4	90.8
γ, °	102.0	101.7	106.5
Resolution range, Å	50–2.40	50–2.10	50–2.22
Unique reflections	47,252 (4,645)	68,018 (6,114)	112,153 (9,155)
Completeness, %	98.4 (96.2)	94.6 (85.5)	92.7 (75.7)
R_{merge}*	0.076 (0.401)	0.049 (0.393)	0.067 (0.321)
Structure solution			
Resolution, Å	2.4		
Se atoms per monomer	3		
Phasing power,† iso/ano	4.51/1.98		
⟨FOM⟩, acentric/centric	0.441/0.339		
⟨FOM⟩ after density modification	0.926		
Refinement			
Resolution, Å	50.0–2.4	50.0–2.1	50.0–2.22
Asymmetric unit	Dimer	Dimer	Two dimers
R value‡	0.226	0.239	0.241
R_{free}	0.239	0.270	0.266
No. of reflections			
R_{work}	42,885	61,400	100,941
R_{free}	1,335	1,940	4,254
σ cutoff	0.0	0.0	0.0
No. of atoms			
Protein	6,978	6,978	13,956
FAD	106	106	212
HEPES	24	—	—
NADPH	—	96	—
Methimazole	—	—	28
Glycerol	—	12	24
Water molecules	382	470	509
rms deviation			
Bond length, Å	0.007	0.008	0.007
Bond angle, °	1.409	1.550	1.380

Data in parentheses represent the outermost shell. ⟨FOM⟩ is the mean figure of merit.

*$R_{sym} = \Sigma_h\Sigma_i|I_i(h) - \langle I(h)\rangle|/\Sigma_h\Sigma_i|I_i(h)|$, where $I_i(h)$ is the intensity measurement for a reflection *h* and $\langle I(h)\rangle$ is the mean intensity for this reflection.

†Phasing power = $\langle F_H\rangle/E$(iso) or $\langle 2F''$ (cal)$\rangle/E$(ano).

‡R value = $\Sigma_i\|F_{i,obs}| - k|F_{i,cal}\|/\Sigma_i|F_{i,obs}|$.

Sequence and Structural Comparison. FMO from *S. pombe* is 30% identical to the FMO of *Saccharomyces cerevisiae* that catalyzes oxidation of biological thiols to maintain the endoplasmic reticulum redox buffer ratio for correct folding of disulfide-bonded proteins (Fig. 8, which is published as supporting information on the PNAS web site) (9, 13). The characteristic sequence motifs, (*i*) FAD binding domain (GXGXXG), (*ii*) NADPH binding domain (GXGXXG), and (*iii*) FMO identifying sequence (FXGXXX-HXXXY/F), are conserved across FMOs (14). However, the NADPH binding motif shows some variation. In the present case it is GGASSA, whereas it is GSSYSA in FMO from *Methylophaga* sp. strain SK1. Sequences of all five human FMOs (FMO1–FMO5) have been compared to that of FMO from *S. pombe* individually, revealing comparable sequence identities of 23.2% to 21.1%. A putative dimethylalanine monooxygenase of human (FMO6) identified recently is 23.6% identical to FMO from *S. pombe* in sequence (15).

Structural comparisons with DALI showed that the fold and topology of this protein resemble those of the oxidoreductases. Structural domain insertion is a common feature among these proteins and is seen in BVMO, NADH peroxidase, and lipoamide dehydrogenase. Although these structures have similar polypeptide chain topologies in general, there are significant differences. FMO has two well defined structural domains, whereas the others have three. The BVMO structure has two structural domains within the insertion in addition to the large domain (16). Other oxidoreductases, such as NADH peroxidase and lipoamide dehydrogenase, have one small insertion domain and two domains, whereas FMO and BVMO have only one domain (17, 18). NADH peroxidase has four domains, including FAD-binding, NAD-binding, central, and interface domains. In this case, the FAD-binding and central domains together resemble the large domain of FMO, and the NAD-binding domain resembles the insertion of FMO. The 60-residue random coil segment running between the large and small domains of FMO is not present in these related proteins.

The flavin portion of the prosthetic group FAD is buried in the BVMO structure; it is in contact with bulk solvent in FMO. This difference may explain why NADPH was not observed in the structure of BVMO when cocrystallized with NADPH (16). Structural differences in the substrate-binding channel almost certainly explain the difference in substrate selectivity of these enzymes. The mechanisms of action of the oxidoreductases are now better understood with the benefit of the FMO structures presented here.

Materials and Methods

Cloning, Expression, and Purification. The cloning and protein production are very similar to those described by Agarwal *et al.* (19). Briefly, the target gene for the protein was amplified via PCR from a *S. pombe* cDNA library with the appropriate forward and reverse primers and TaqDNA polymerase (Qiagen) using standard methods. After gel purification, the PCR product was inserted into a

modified pET26b vector for topoisomerase-directed cloning (Invitrogen) designed to express the protein with a C-terminal hexahistidine tag and transformed into BL21 (DE3) cells. The clone was confirmed for correct sequence. The expression and solubility were tested by standard methods. The protein yield was 75.1 mg, which was concentrated to 45.1 mg/ml. Selenomethionine-labeled protein was produced and purified in a similar manner.

FMO Activity. The enzymatic assay for measuring FMO activity of the wild-type protein was performed by using the most common substrate, methimazole (1). A final volume of assay mixture (100 μl) contained 100 mM tricine buffer, 1 mM EDTA, 0.4 mg of protein sample, 0.1 mM NADPH, 0.02 mM DTT, and 0.06 mM DTNB in 6.0 mM phosphate buffer. FMO activity was evaluated by spectrophotometric measurement of OD at 412 nm after addition of methimazole.

Structure Determination of Enzyme–FAD Complex. Purified protein in 10 mM Hepes (pH 7.0) plus 150 mM NaCl was used for crystallization. Diffraction-quality crystals were obtained by sitting drop-vapor diffusion against a reservoir containing 20% PEG 4000 and 0.1 M sodium citrate buffer (pH 5.8) with 1,6-diaminohexane as additive. The same crystallization condition was used for the SeMet protein. Cryoprotection was achieved by addition of glycerol to a final concentration of 10% (vol/vol). X-ray diffraction data were collected under standard cryogenic conditions at beamline X25 of the National Synchrotron Light Source at Brookhaven National Laboratory. Crystals belonged to the space group P1 with two molecules in the unit cell and diffracted to 2.4-Å resolution. The structure was determined by the three-wavelength multi-wavelength anomalous dispersion method. Se positions were determined by using SOLVE (20). Refinement of the Se positions, phase refinement and extension, and density modification were performed by using SHARP and DM (21, 22). The experimental electron density map calculated with phases from SHARP showed clear secondary structure elements. Automatic model building was attempted with ARP/WARP (23), which built 84% of the polypeptide chain without manual intervention. Model building was completed manually by using O (24).

The structure was refined by using CNS 1.1 (25). Interpretable electron density features were observed for the prosthetic group FAD, water molecules, and a buffer component Hepes, which were included in the final refinements. Data collection and refinement parameters are provided in Table 3.

Structure Determination of Enzyme–FAD–NADPH Complex. Purified protein was incubated with NADPH in a 1:5 molar ratio for 30 min at room temperature before crystallization trials. Crystals were obtained under the same conditions as for the enzyme–FAD complex and belong to the same crystal form. The isomorphous structure was determined by difference Fourier synthesis using the enzyme–FAD complex as a phasing model and refined to convergence with CNS 1.1. A composite omit map showed unambiguously interpretable electron density for the cofactor NADPH. Further refinement was carried out after addition of NADPH, water molecules, and a glycerol molecule (located at the binding site for the Hepes molecule seen in the enzyme–FAD complex structure). Refinement statistics are presented in Table 3.

Structure Determination of Enzyme–FAD–Methimazole Complex. The enzyme–FAD–NADPH complex was prepared as before and incubated for 1 h at room temperature with 5-fold molar excess of methimazole. Crystals grew under the same conditions as before, and x-ray diffraction data were collected under identical conditions. These crystals belong to the same space group (P1), but the unit cell dimensions differ from those obtained with the enzyme–FAD complex crystals, giving four molecules per unit cell. The structure was determined by molecular replacement using the enzyme–FAD complex as a search model (26). A composite omit map showed residual electron density for FAD and methimazole only. NADPH was not observed in the crystal structure. Water molecules and one glycerol per monomer were added, and the refinement was completed (Table 3).

Sequence and Structural Comparisons. Primary structure comparisons were performed initially by BLAST, and sequentially similar proteins were identified (27). One-to-one comparison of selected proteins was performed by CLUSTALW (28). Multiple sequence alignment of a set of selected proteins was done by T-COFFEE (29). Three-dimensional structure of the FMO was compared with other structures using the DALI server to detect protein fold similarity (30).

We thank Dr. Kumaran for helpful discussions. Research was supported by National Institutes of Health Grant GM62529 to the New York SGX Research Consortium under Department of Energy Prime Contract DEAC02-98CH10886 to Brookhaven National Laboratory.

1. Dixit, A. & Roche, T. E. (1984) *Arch. Biochem. Biophys.* **233,** 50–63.
2. Poulsen, L. L. & Ziegler, D. (1979) *J. Biol. Chem.* **254,** 6449–6455.
3. Fraaije, M. W., Kamerbeek, N. M., van-Berkel, W. J. J. & Janssen, D. B. (2002) *FEBS Lett.* **518,** 43–47.
4. Ziegler, D. M. (1993) *Annu. Rev. Pharmocol. Toxicol.* **33,** 179–199.
5. Cashman, J. R. (2000) *Curr. Drug Metab.* **1,** 181–191.
6. Cashman, J. R. (2004) *Drug Discovery Today* **9,** 574–581.
7. Treacy, E. P., Akerman, B. R., Chow, L. M. L., Youil, R., Bibeau, C., Lin, J., Bruce, A. G., Knight, M., Danks, D. M., Cashman, J. R., *et al*. (1998) *Hum. Mol. Genet*. **7,** 839–845.
8. Wood, V., Gwilliam, R., Rajandream, M. A., Lyne, M., Lyne, R., Stewart, A., Sgouros, J., Peat, N., Hayles, J., Baker, S., *et al*. (2002) *Nature* **415,** 871–880.
9. Suh, J. K., Poulsen, L. L., Ziegler, D. M. & Robertus, J. D. (1996) *Arch. Biochem. Biophys.* **336,** 268–274.
10. Karlsson, A., Parales, J. V., Parales, R. E., Gibson, D. T., Eklund, H. & Ramaswamy, S. (2003) *Science* **299,** 1039–1042.
11. Wilmot, C. M., Hajdu, J., McPherson, M. J., Knowles, P. F. & Phillips, S. E. (1999) *Science* **286,** 1724–1728.
12. Schlichting, I., Berendzen, J., Chu, K., Stock, A. M., Maves, S. A., Benson, D. E., Sweet, R. M., Ringe, D., Petsko, G. A. & Sligar, S. G. (2000) *Science* **287,** 1615–1622.
13. Goffeau, A., Barrell, B. G., Bussey, H., Davis, R. W., Dujon, B., Feldmann, H., Galibert, F., Hoheisel, J. D., Jacq, C., Johnston, M., *et al*. (1996) *Science* **274,** 546, 563–567.
14. Choi, H. S., Kim, J. K., Vho, E. H., Kim, Y. C., Kim, J. I. & Kim, S. W. (2003) *Biochem. Biophys. Res. Commun.* **306,** 930–936.
15. Furnes, B., Feng, J., Sommer, S. S. & Schlenk, D. (2003) *Drug Metab. Dispos.* **31,** 187–193.
16. Malito, E., Alfieri, A., Fraaije, M. W. & Mattevi, A. (2004) *Proc. Natl. Acad. Sci. USA* **101,** 13157–13162.
17. Mattevi, A., Obmolova, G., Sokatch, J. R., Betzel, C. & Hol, W. G. J. (1992) *Proteins Struct. Funct. Genet.* **13,** 336–351.
18. Stehle, T., Ahmed, S. A., Claiborne, A. & Schulz, G. E. (1991) *J. Mol. Biol.* **221,** 1325–1344.
19. Agarwal, R., Bonanno, J. B., Burley, S. K. & Swaminathan, S. (2006) *Acta Crystallogr. D* **62,** 383–391.
20. Terwilliger, T. C. & Berendzen, J. (1997) *Acta Crystallogr. D* **55,** 849–861.
21. Cowtan, K. D. & Main, P. (1996) *Acta Crystallogr. D* **52,** 43–48.
22. de La Fortelle, E. & Bricogne, G. (1997) *Methods Enzymol.* **276,** 472–493.
23. Perrakis, A., Morris, R. & Lamzin, V. S. (1999) *Nat. Struct. Biol.* **6,** 458–463.
24. Jones, T. A., Zou, J., Cowtan, S. & Kjeldgaard, M. (1991) *Acta Crystallogr. A* **47,** 110–119.
25. Brunger, A. T., Adams, P. D., Clore, G. M., Delano, W. L., Gros, P., Grosse-Kunstleve, R. W., Jiang, J. S., Kuszewski, J., Nilges, M., Pannu, N. S., *et al*. (1998) *Acta Crystallogr. D* **54,** 905–921.
26. Vagin, A. & Teplyakov, A. (2000) *Acta Crystallogr. D* **56,** 1622–1624.
27. Altschul, S. F., Madden, T. L., Schaffer, A. A., Zhang, J., Zhang, Z., Miller, W. & Lipman, D. J. (1997) *Nucleic Acids Res.* **25,** 3389–3402.
28. Thompson, J. D., Higgins, D. G. & Gibson, T. J. (1994) *Nucleic Acids Res.* **22,** 4673–4680.
29. Notredame, C., Higgins, D. G. & Heringa, J. (2000) *J. Mol. Biol.* **302,** 205–217.
30. Holm, L. & Sander, C. (1993) *J. Mol. Biol.* **233,** 123–138.